

Dissipation induced macroscopic entanglement in an open optical lattice

G. Kordas,^{1,2} S. Wimberger,¹ and D. Witthaut³

¹*Institut für theoretische Physik and Center for Quantum Dynamics, Universität Heidelberg, Heidelberg, Germany*

²*University of Athens, Physics Department, Panepistimiopolis, Ilissia 15771 Athens, Greece*

³*Network Dynamics, Max Planck Institute for Dynamics and Self-Organization, D-37077 Göttingen, Germany*

We introduce a method for the dissipative preparation of strongly correlated quantum states of ultracold atoms in an optical lattice via localized particle loss. The interplay of dissipation and interactions enables different types of dynamics. This ushers a new line of experimental methods to maintain the coherence of a Bose-Einstein condensate or to deterministically generate macroscopically entangled quantum states.

PACS numbers: 03.67.Gg, 03.65.Yz, 03.75.Lm

I. INTRODUCTION

Decoherence and dissipation, caused by the irreversible coupling of a quantum system to its environment, represent a major obstacle for a long-time coherent control of quantum states. Sophisticated methods have been developed to maintain coherence in open quantum systems with applications in quantum control and quantum information processing [1, 2]. Only recently a new paradigm has been put forward: Dissipation can be used as a powerful tool to steer the dynamics of complex quantum systems if it can be accurately controlled. It was shown that dissipative processes can be tailored to prepare arbitrary pure states [3, 4] or to enable universal quantum computation [5]. Several methods have been proposed to dissipatively generate entangled states [6, 7]. However, most proposals rely on rather special dissipation processes, such that a sophisticated control of the coupling of system and environment must be realized.

In this letter we propose a scheme to create macroscopically entangled quantum states of ultracold atoms based on localized particle loss. This process can be readily realized in ongoing experiments with optical lattices enabling a single-site access [8–13]. The generated quantum states show remarkable statistical properties: The atoms relax to a coherent superposition of bunches localized at different lattice positions. These states generalize the so-called NOON states enabling interferometry beyond the standard quantum limit [14, 15]. Furthermore, they may serve as a distinguished probe of decoherence and the emergence of classicality. As particle loss is an elementary and omnipresent dissipation process, this method may be generalized to a variety of open quantum systems well beyond the dynamics of ultracold atoms.

II. PARTICLE LOSS IN AN OPTICAL LATTICE

The coherent dynamics of bosonic atoms in an optical lattice is described by the Bose-Hubbard Hamiltonian [16]

$$\hat{H} = -J \sum_j \left(\hat{a}_{j+1}^\dagger \hat{a}_j + \hat{a}_j^\dagger \hat{a}_{j+1} \right) + \frac{U}{2} \sum_j \hat{a}_j^\dagger \hat{a}_j^\dagger \hat{a}_j \hat{a}_j, \quad (1)$$

where \hat{a}_j and \hat{a}_j^\dagger are the bosonic annihilation and creation operators in the j th well. We set $\hbar = 1$, thus measuring all energies in frequency units. Throughout this letter we assume periodic boundary conditions.

We analyze the dynamics of ultracold atoms induced by particle loss from a single lattice site acting in concurrence with strong atom-atom interactions. Single site access can be implemented optically either by increasing the lattice period [8, 9] or by pushing the resolution of the optical imaging system to the limit [10, 11]. Detection and coherent manipulation of the atoms with off-resonant light have been demonstrated, whereas a controllable particle loss can be implemented with a strong resonant blast laser in a straightforward way. An even higher resolution can be realized by a focussed electron beam ionizing atoms which are then removed from the lattice [12, 13]. This can be used for the detection of single atoms as well as for an incoherent manipulation of the quantum dynamics in the lattice [17–19].

In addition to this tunable source of dissipation, phase noise can limit the coherence in the lattice [20–23]. The dynamics of the atoms is then described by a quantum master equation [2, 18, 19, 24, 25]

$$\begin{aligned} \dot{\hat{\rho}} = & -i[\hat{H}, \hat{\rho}] - \frac{\kappa}{2} \sum_{j=1,2} (\hat{n}_j^2 \hat{\rho} + \hat{\rho} \hat{n}_j^2 - 2\hat{n}_j \hat{\rho} \hat{n}_j) \\ & - \frac{1}{2} \sum_j \gamma_j \left(\hat{a}_j^\dagger \hat{a}_j \hat{\rho} + \hat{\rho} \hat{a}_j^\dagger \hat{a}_j - 2\hat{a}_j \hat{\rho} \hat{a}_j^\dagger \right), \quad (2) \end{aligned}$$

where γ_j is the loss rate at the j th site, $\hat{n}_j = \hat{a}_j^\dagger \hat{a}_j$ are the number operators and κ is the rate of phase noise. We analyze the effects of decoherence in Fig. 2, otherwise we set $\kappa = 0$. Numerical simulations are carried out using the quantum jump method [26] for small systems and the truncated Wigner method [27] for large lattices.

III. DISSIPATION INDUCED MACROSCOPIC ENTANGLEMENT

We first consider the dynamics of ultracold atoms in a triple-well trap as illustrated in Fig. 1 (a), where a numerically exact solution is still possible for reasonable

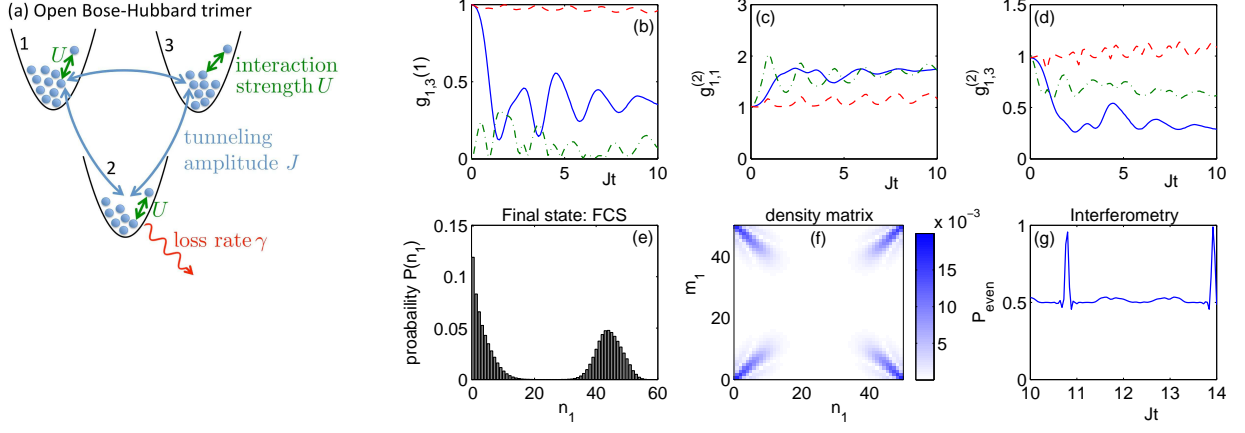


FIG. 1: Dissipative generation of a macroscopically entangled breather state in an open Bose-Hubbard trimer. (a) Schematic drawing of the system. (b) Evolution of the phase coherence $g_{1,3}^{(1)}(t)$ for the symmetric initial state $|\Psi_+\rangle$ (dashed line), the anti-symmetric initial state $|\Psi_-\rangle$ (solid line), and the Fock state $|\Psi_F\rangle$ (dash-dotted line). (c,d) Evolution of the number fluctuations $g_{1,1}^{(2)}(t)$ and correlations $g_{1,3}^{(2)}(t)$. (e,f) Analysis of the final state at $t = 10J^{-1}$ for the anti-symmetric initial state $|\Psi_-\rangle$. (e) The full counting statistics in the first well. (f) The density matrix elements $\rho(n_1, 0, n - n_1; m_1, 0, n - m_1)$ for $n = 50$ reveals the coherence of the breather state. (g) Matter wave interferometry of the breather state. Plotted is the probability to detect an even number of atoms at site 1. Parameters are $U = 0.1J$, $\gamma_2 = 0.2J$, $\gamma_1 = \gamma_3 = 0$ and $N(0) = 60$.

atom numbers. We analyze the quantum state of the atoms characterized by the correlation functions

$$g_{j,\ell}^{(1)} = \frac{\langle \hat{a}_j^\dagger \hat{a}_\ell \rangle}{\sqrt{\langle \hat{n}_j \rangle \langle \hat{n}_\ell \rangle}} \quad \text{and} \quad g_{j,\ell}^{(2)} = \frac{\langle \hat{n}_j \hat{n}_\ell \rangle}{\langle \hat{n}_j \rangle \langle \hat{n}_\ell \rangle}. \quad (3)$$

The first-order correlation function $g^{(1)}$ measures the phase coherence between two wells, while $g^{(2)}$ gives the number fluctuations or number correlations between different wells. The evolution of these functions is plotted in Fig. 1 (b-d) for three different initial states, a pure Bose-Einstein condensate (BEC) with (anti)symmetric wave function $|\Psi_\pm\rangle \sim (\hat{a}_1^\dagger \pm \hat{a}_3^\dagger)^N |0, 0, 0\rangle$ and a Fock state $|\Psi_F\rangle = |N/2, 0, N/2\rangle$, respectively. In all cases we assume strong atom-atom interactions $U = 0.1J$, such that $UN > J$. For the symmetric initial state $|\Psi_+\rangle$, all correlations remain close to the initial values indicating that the BEC remains approximately pure for all times. More precisely, the quantum state is approximately given by a superposition of pure product states $|\Psi_n\rangle = |\psi_1\rangle^{\otimes n}$ with different atom numbers n , where all atoms occupy the same single-particle state $|\psi_1\rangle$. The atoms decay from the lattice in an uncorrelated way, which is well described by mean-field theory [18, 19]. Another more subtle effect is that localized particle loss can maintain or even restore the purity of a condensate as non-condensed atoms are rapidly removed from the lattice [28, 29].

In contrast, the anti-symmetric initial state $|\Psi_-\rangle$ is dynamically unstable such that the condensate is rapidly destroyed and phase coherence is lost. The nature of the emerging quantum state is revealed by the $g^{(2)}$ -function: Number fluctuations strongly increase while the correlations decrease. This shows that the atoms start to bunch at one lattice site while the other sites are essentially

empty. A similar dynamics is found for the Fock state $|\Psi_F\rangle$, however the number anti-correlations are less pronounced and the equilibration to the final state takes a longer time. The emerging state is called a breather state in the following in analogy to localized modes in nonlinear lattices [30, 31].

The full counting statistics of the atoms shown in Fig. 1 (e) clearly reveals that the atoms relax either to site 1 or to site 3, leaving site 2 essentially empty. Most interestingly, these two contributions are phase coherent, which is confirmed by an analysis of the density matrix of the atoms. Figure 1 (f) shows the matrix elements $\rho(n_1, 0, n - n_1; m_1, 0, n - m_1)$ for $n = 50$, the most probable value of the atom number at $t = 10J^{-1}$. Full coherence is observed between the contributions with small and large atom number at site 1, i.e. $n_1 \geq 0$ and $n_1 \leq 50$.

The breather states generated by this protocol generalize the so-called NOON states $|n, 0, 0\rangle + e^{i\vartheta} |0, 0, n\rangle$ which enable precision interferometry beyond the standard quantum limit [15]. Breather states can be written as a superposition of states of the form

$$|n_1, n_2, n - n_1 - n_3\rangle + e^{i\vartheta} |n - n_1 - n_3, n_2, n_1\rangle. \quad (4)$$

The number of atoms n varies, but the coherence of wells 1 and 3 is guaranteed, which is sufficient for precision interferometry. We consider an interferometric measurement, where the modes (lattice sites) 1 and 3 are mixed as given by the time evolution operator $\hat{U} = \exp(-i\hat{H}_{\text{mix}}t)$ with $\hat{H}_{\text{mix}} = iJ(\hat{a}_1^\dagger \hat{a}_3 - \hat{a}_3^\dagger \hat{a}_1)$, assuming that interactions and loss are switched off. In analogy to the parity observable [14], we record the probability $P_{\text{even}}(t)$ to detect an even number of atoms in lattice site 1, which is shown as a function of time in Fig. 1 (g). We find that

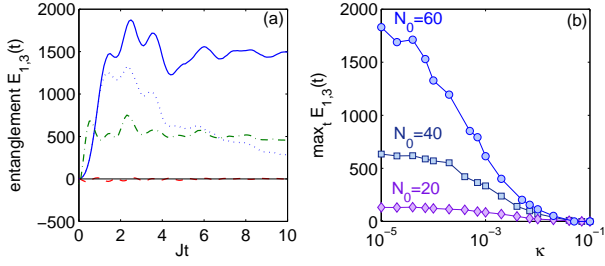


FIG. 2: Entanglement and decoherence of a breather state in a triple-well trap. (a) Evolution of the entanglement parameter (5) for $\kappa = 0$ and three different initial states, $|\Psi_+\rangle$ (dashed line), $|\Psi_-\rangle$ (solid line), and $|\Psi_F\rangle$ (dash-dotted line), and for $|\Psi_-\rangle$ in the presence of modest phase noise, $\kappa = 10^{-4}J$ (dotted line) and $N(0) = 60$. (b) Maximum of the entanglement parameter $\max_t E_{1,3}(t)$ as a function of the noise rate κ for the anti-symmetric initial state $|\Psi_-\rangle$ and different particle numbers. The remaining parameters are the same as in Fig. 1.

P_{even} approaches unity periodically, which proves that the breather states are fully phase coherent and thus enable quantum interferometry as ordinary NOON states. Breather states are readily generated for large particle numbers, which is notoriously difficult using other methods (see, e.g., [32]).

IV. ENTANGLEMENT AND DECOHERENCE

The atoms in a breather or NOON state are strongly entangled: If some atoms are measured at one site, then the remaining atoms will be projected to the same site with overwhelming probability. To unambiguously detect this form of multi-partite entanglement, we analyze the variance of the population imbalance $\Delta(\hat{n}_3 - \hat{n}_1)^2$, which scales as $\sim N^2$ for a breather state, while it is bounded by N for a pure product state, N being the total atom number. Given a pure state decomposition of the quantum state $\hat{\rho} = L^{-1} \sum_{a=1}^L |\psi_a\rangle \langle \psi_a|$, we introduce the entanglement parameter

$$E_{j,k} := \langle (\hat{n}_j - \hat{n}_k)^2 \rangle - \langle \hat{n}_j - \hat{n}_k \rangle^2 - \langle \hat{n}_j + \hat{n}_k \rangle - \frac{1}{2L^2} \sum_{a,b} [\langle \hat{n}_j - \hat{n}_k \rangle_a - \langle \hat{n}_j - \hat{n}_k \rangle_b]^2,$$

for the wells (j,k) , where $\langle \cdot \rangle_{a,b}$ denotes the expectation value in the pure state $|\psi_{a,b}\rangle$. Such a pure state decomposition is automatically provided by a quantum jump simulation [26]. The last term in the parameter E corrects for the possibility of an incoherent superposition of states localized at sites 1 and 3. For a separable quantum state one can show that $E_{j,k} < 0$ such that a value $E_{j,k} > 0$ unambiguously proves entanglement of the atoms. A proof is given in the appendix.

As shown in Fig. 2 (a), $E_{1,3}(t)$ rapidly relaxes to a large non-zero value for a Fock or an anti-symmetric initial state, which is maintained during the full duration

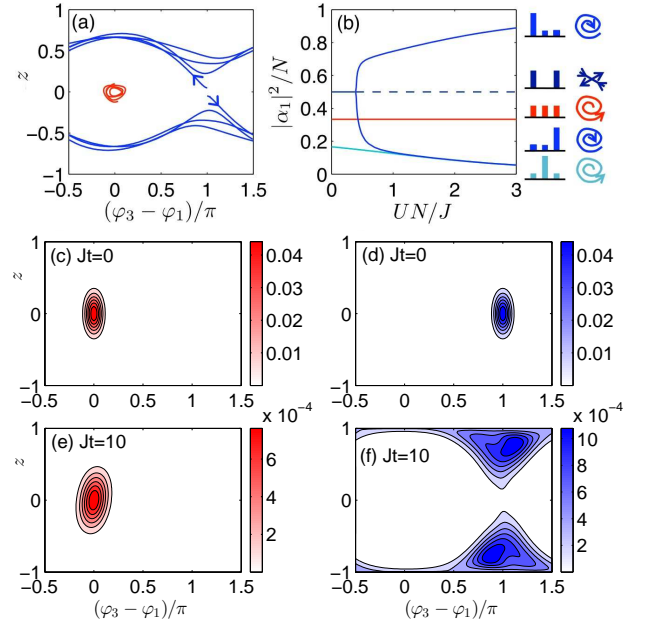


FIG. 3: Semiclassical interpretation of breather state formation. (a) Classical trajectories starting close to the symmetric state $(\alpha_1, \alpha_2, \alpha_3) = (1, 0, 1)/\sqrt{2}$ (red) and the anti-symmetric state $(1, 0, -1)/\sqrt{2}$ (blue). (b) Meta-stable classical states as a function of the interaction strength. Plotted is the relative occupation at site 1. The icons on the right illustrate the population at the three sites and the dynamical stability of these states. Breathers emerge for $UN > 0.4J$, N being the total atom number. (c-f) The quantum dynamics of the Q function follows the classical phase space trajectories. (c,e) A BEC with a symmetric wave function $|\Psi_+\rangle$ remains approximately pure. (d,f) A BEC with an anti-symmetric wave function $|\Psi_-\rangle$ is coherently split into two parts forming the breather state. The Husimi function $Q(\alpha_1, \alpha_2, \alpha_3)$ is plotted as a function of the population imbalance $z = (|\alpha_3|^2 - |\alpha_1|^2)/N$ and the relative phase $\phi_3 - \phi_1$ for $\alpha_2 = 0$ and $|\alpha_1|^2 + |\alpha_3|^2 = N$. Parameters as in Fig. 1.

of the simulation. This proves the deterministic generation of a meta-stable macroscopically entangled quantum state by localized particle dissipation. Furthermore, entangled breather states provide a sensitive probe for environmentally induced decoherence. Figure 2 (b) shows the maximum value of $E_{1,3}(t)$ realized in the presence of phase noise. Entanglement decreases with the noise rate κ , in which breather states with large particle numbers are most sensitive. However, entanglement persists up to relatively large values of $\kappa \approx 10^{-2}J$ in all cases.

V. SEMICLASSICAL INTERPRETATION

The formation of breather states can be understood to a large extent within a semi-classical phase space picture. Any quantum state can be represented by a quasi distribution function on the associated classical phase space without loss of information [2]. In the following, we con-

sider the Husimi function defined as $Q(\alpha_1, \alpha_2, \alpha_3; t) = \langle \alpha_1, \alpha_2, \alpha_3 | \hat{\rho}(t) | \alpha_1, \alpha_2, \alpha_3 \rangle$, where $|\alpha_j\rangle$ is a Glauber coherent state in the j th well. The dynamics of these distribution functions is to leading order given by a classical Liouville equation,

$$\frac{\partial Q}{\partial t} = - \sum_j \left(\frac{\partial}{\partial \alpha_j} \dot{\alpha}_j + \frac{\partial}{\partial \alpha_j^*} \dot{\alpha}_j^* \right) Q + \text{noise}. \quad (6)$$

Therefore the ‘classical’ flow provides the skeleton of the quantum dynamics of the Husimi function, whereas the quantum corrections vanish with increasing particle number as $1/N$ [33]. Figure 3 (a) illustrates the ‘classical’ dynamics which is given by the dissipative discrete Gross-Pitaevskii equation (DGPE)

$$i\dot{\alpha}_j = -J(\alpha_{j+1} - \alpha_{j-1}) + U|\alpha_j|^2\alpha_j - i\gamma_j\alpha_j/2. \quad (7)$$

The figure shows the evolution of the population imbalance $z = (|\alpha_3|^2 - |\alpha_1|^2)/N$ and the relative phase $\Delta\varphi = \varphi_3 - \varphi_1$, where $\alpha_j = |\alpha_j|e^{i\varphi_j}$, for three different initial values. The trajectory with $\Delta\varphi = 0$ (red) is dynamically stable, such that it remains in the vicinity of the point $(z, \Delta\varphi) = (0, 0)$ for all times. In contrast, trajectories starting close to $(z, \Delta\varphi) = (0, \pi)$ converge to regions with either $z > 0$ or $z < 0$. These regions correspond to self-trapped states, which are known from the non-dissipative case [8, 34, 35]. For $\gamma_2 > 0$, these states become *attractively stable*, which enables the dynamic formation of breather states. Self-trapping occurs only if the interaction strength exceeds the critical value $U_{\text{cr}} = 0.4 J N^{-1}$ for the bifurcation shown in Fig. 3 (b). The anti-symmetric state $(z, \Delta\varphi) = (0, \pi)$ becomes unstable, whereas two attractively stable self-trapping states emerge. The symmetric state remains marginally stable for all values of U .

The corresponding quantum dynamics is shown in Fig. 3 (c-f). The Husimi functions of the symmetric initial state $|\Psi_+\rangle$ and the anti-symmetric initial state $|\Psi_-\rangle$ are localized around $(z, \Delta\varphi) = (0, 0)$ and $(z, \Delta\varphi) = (0, \pi)$, respectively, as shown in Fig. 3 (c,d). As predicted by the DGPE, the symmetric state $|\Psi_+\rangle$ remains localized around $(z, \Delta\varphi) = (0, 0)$ for all times. On the contrary, the Husimi function of the anti-symmetric state $|\Psi_-\rangle$ flows to the self-trapping regions, such that the final state is a superposition of two fragments with $z > 0$ and $z < 0$ – a breather state (cf. Fig. 3 (e)). The semi-classical picture predicts the fragmentation of the condensate but, of course, cannot assert the coherence and thus the entanglement of the fragments which is a genuine quantum feature. However, it correctly predicts the critical interaction strength for the emergence of breather states.

VI. EXTENDED LATTICES

The entanglement protocol can be straightforwardly generalized to extended optical lattices, such that a realization is readily possible in ongoing experiments. First,

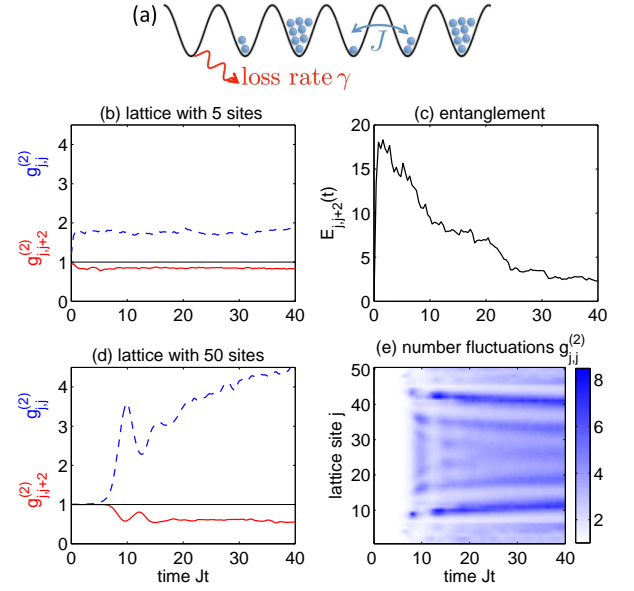


FIG. 4: Generation of breather states in an optical lattice by localized atom loss. (a) Scheme of a possible experiment. (b,d) The presence of large number fluctuations $g_{j,j}^{(2)}(t) > 1$ (dashed blue lines) and anti-correlations $g_{j,j+2}^{(2)}(t) < 1$ (solid red lines) indicates a breather state. (c) The criterion $E_{j,j+2} > 0$ unambiguously proves the entanglement of the atoms (cf. Eq. (5)). (e) The number fluctuations $g_{j,j}^{(2)}(t)$ increase after a short transient period for all lattice sites j in a similar way. Results are shown for (b,c) a small lattice with $M = 5$ sites and $j = 3$, $U = J$, $\gamma_1 = 0.2J$, and $N(0) = 16$ (solid lines) and (d,e) an extended lattice with $M = 50$ sites and $j = 25$, $UN(0) = 25J$, $\gamma_1 = 2J$, and $N(0)/M = 1000$ (dashed lines). The initial state is a pure BEC prepared at the band edge.

a BEC is moved at constant speed [36] or accelerated [37] to the edge of the first Brillouin zone such that the quantum state of the atoms at $t = 0$ is given by $|\Psi(0)\rangle \sim (\sum_j \psi_j \hat{a}_j^\dagger)^N |0\rangle$ with $\psi_j \sim (-1)^j$. Then the atoms evolve freely according to the Master equation (2) subject to particle loss from lattice site $j = 1$ as illustrated in Fig. 4 (a). We simulate the dynamics for a small lattice with $M = 5$ sites and for an extended lattice with $M = 50$ assuming periodic boundary conditions. In the latter case we use the truncated Wigner method [27], which is especially suited for the large filling factors considered here and describes the deviation from a pure BEC state in contrast to a simple mean-field approach.

As a fingerprint for the dynamical generation of breather states we analyze the evolution of the number correlation functions as shown in Fig. 4 (b,d). After a short period of equilibration, the number fluctuations strongly increase, while the number correlations to the next-to-nearest neighboring site decrease. A similar picture emerges if we plot the $g_{j,j}^{(2)}$ functions for different lattice sites as in Fig. 4 (e). As above, this fact shows that the atoms start to bunch in one or more breathers while

the remaining lattice sites are essentially empty. In large lattices, breathers generally extend over more than one lattice site, such that anti-correlations $g_{j,k}^{(2)} < 1$ are observed only for the next-to-nearest neighbors $|j - k| \geq 2$. The position of these breathers is random due to quantum fluctuations. Hence, the final quantum state is a superposition of breathers at different sites, a macroscopically entangled state. The rapid increase of the entanglement parameter (5) shown in Fig. 4 (c) unambiguously proves the presence of many-particle entanglement for a small lattice with five sites. For long times $E_{3,5}(t)$ tends to zero again, simply because all atoms have decayed from the lattice. Breathers appear only when the interaction strength Un exceeds a critical value, which can be inferred from semiclassical arguments. This transition can be interpreted as a dynamical phase transition [31] and will be analyzed in detail in a forthcoming article [38].

VII. CONCLUSION

Engineering dissipation is a promising new direction in the control of complex quantum systems. We have shown that an elementary dissipation process, the localized loss of particles, together with repulsive interactions, is sufficient to create macroscopically entangled states of ultracold atoms in optical lattices. The quantum state is a coherent superposition of atoms bunched at different lattice sites. We have discussed the properties of these ‘breather states’ in detail, including entanglement, decoherence and applications in precision quantum interferometry. A semiclassical interpretation of breather state formation has revealed the connection to a classical bifurcation of the associated mean-field dynamics.

Breather states are significantly different from squeezed entangled states, where interactions reduce (‘squeeze’) the number variance in a well of the lattice [9, 39]. In a breather state, a well is either occupied by a large number of atoms or empty, giving rise to a large number variance. The entanglement enables precision metrology beyond the standard quantum limit using protocols introduced for optical NOON states.

The introduced protocol can be readily implemented experimentally with ultracold atoms in optical lattices. Localized access to the lattice can be realized either optically or by a focussed electron beam [8–13]. Macroscopically entangled breather states are then formed dynamically as meta-stable states of the dissipative quantum dynamics. This protocol is very favorable as no fine-tuning of parameters is needed and the entanglement persists as long as enough atoms remain in the lattice. As particle loss is an elementary dissipation process, the effects discussed here may be important for a variety of different physical systems, as for instance, optical fiber experiments [40].

We thank O. G  hne for stimulating discussions. We acknowledge financial support by the Max Planck Soci-

ety, the Deutsche Forschungsgemeinschaft via FOR760, the individual grant WI 3426/3-1 and the HGSFP (GSC 129/1).

VIII. APPENDIX

In this appendix we present a detailed derivation of the entanglement criterion (5). This result generalizes established entanglement criteria in terms of spin squeezing [39] and is derived in a similar way. In contrast to spin squeezing inequalities, it shows that a state is entangled if the variance (5), defined in the text, is *larger* than a certain threshold value. We assume that the many-body quantum state $\hat{\rho}$ is decomposed into a mixture of pure states

$$\hat{\rho} = \sum_a p_a \hat{\rho}_a = \sum_a p_a |\psi_a\rangle \langle \psi_a|, \quad (8)$$

where every pure state $\hat{\rho}_a = |\psi_a\rangle \langle \psi_a|$ has a fixed particle number N_a . Now we prove that the entanglement parameter (5) is negative, $E_{j,k} < 0$, for every separable state such that a value $E_{j,k} > 0$ unambiguously reveals the presence of many-particle entanglement.

We start with pure states $\hat{\rho}_a$. If such a pure state $\hat{\rho}_a$ is separable, it can be written as a tensor product of single particle states

$$\hat{\rho}_a = \hat{\rho}_a^{(1)} \otimes \hat{\rho}_a^{(2)} \otimes \dots \otimes \hat{\rho}_a^{(N_a)}. \quad (9)$$

We furthermore introduce the abbreviation $\hat{S}_{\pm} := \hat{n}_j \pm \hat{n}_k$. This operator is also written as a tensor product of single-particle operators

$$\hat{S}_{\pm} = \sum_{r=1}^N \mathbb{1} \otimes \dots \otimes \mathbb{1} \otimes \hat{s}_{\pm}^{(r)} \otimes \mathbb{1} \otimes \dots \otimes \mathbb{1}, \quad (10)$$

where the superscript (r) denotes that the single-particle operator $\hat{s}_{\pm}^{(r)}$ acts on the r th atom. The single-particle operators are given by $\hat{s}_{\pm} = |j\rangle \langle j| \pm |k\rangle \langle k|$, where $|j\rangle$ is the quantum state where the particle is localized in site j .

For a separable pure state $\hat{\rho}_a$, the expectation values of the population imbalance $\langle \hat{S}_{-} \rangle_a = \text{tr}[\hat{\rho}_a \hat{S}_{-}]$ and its

square can be expressed as

$$\langle \hat{S}_- \rangle = \sum_{r=1}^N \text{tr} \left[\rho^{(r)} \hat{s}_-^{(r)} \right], \quad (11)$$

$$\begin{aligned} \langle \hat{S}_-^2 \rangle &= \sum_{r \neq q}^N \text{tr} \left[(\rho^{(r)} \otimes \rho^{(q)}) (\hat{s}_-^{(r)} \otimes \hat{s}_-^{(q)}) \right] \\ &\quad + \sum_{r=1}^N \text{tr} \left[\rho^{(r)} \hat{s}_-^{(r)2} \right] \\ &= \sum_{r,q=1}^N \text{tr} \left[\rho^{(r)} \hat{s}_-^{(r)} \right] \text{tr} \left[\rho^{(q)} \hat{s}_-^{(q)} \right] \\ &\quad - \sum_{r=1}^N \text{tr} \left[\rho^{(r)} \hat{s}_-^{(r)} \right] \text{tr} \left[\rho^{(r)} \hat{s}_-^{(r)} \right] + \sum_{r=1}^N \text{tr} \left[\rho^{(r)} \hat{s}_-^{(r)2} \right] \\ &= \langle \hat{S}_- \rangle^2 + \sum_{r=1}^N \text{tr} \left[\rho^{(r)} \hat{s}_-^{(r)2} \right] - \left\{ \text{tr} \left[\rho^{(r)} \hat{s}_-^{(r)} \right] \right\}^2. \end{aligned} \quad (12)$$

Using $\text{tr}[\rho^{(r)} \hat{s}_-^{(r)2}] = \text{tr}[\rho^{(r)} \hat{s}_+^{(r)}]$ we thus find that every pure products state $\hat{\rho}_a$ satisfies the condition

$$\langle \hat{S}_-^2 \rangle_a - \langle \hat{S}_- \rangle_a^2 \leq \langle \hat{S}_+ \rangle_a. \quad (13)$$

If the total quantum state $\hat{\rho}$ is separable, such that it can be written as a mixture of separable pure states (8), the expectation values are given by

$$\begin{aligned} \langle \hat{S}_-^2 \rangle &= \sum_a p_a \langle \hat{S}_-^2 \rangle_a \leq \langle \hat{S}_+ \rangle + \sum_a p_a \langle \hat{S}_- \rangle_a^2 \\ \langle \hat{S}_- \rangle^2 &= \sum_{a,b} p_a p_b \langle \hat{S}_- \rangle_a \langle \hat{S}_- \rangle_b \\ &= \sum_a p_a \langle \hat{S}_- \rangle_a^2 - \frac{1}{2} \sum_{a,b} p_a p_b \left[\langle \hat{S}_- \rangle_a - \langle \hat{S}_- \rangle_b \right]^2. \end{aligned} \quad (14)$$

We thus find that every separable quantum state satisfies the following inequality for the variance of the population imbalance \hat{S}_- :

$$\langle \hat{S}_-^2 \rangle - \langle \hat{S}_- \rangle^2 \leq \langle \hat{S}_+ \rangle + \frac{1}{2} \sum_{a,b} p_a p_b \left[\langle \hat{S}_- \rangle_a - \langle \hat{S}_- \rangle_b \right]^2. \quad (15)$$

This inequality for separable states can be rewritten as $E_{j,k} < 0$ in terms of the entanglement parameter (5).

-
- [1] Nielsen M. A. and Chuang I. L., *Quantum Computation and Quantum Information* (Cambridge University Press, Cambridge) 2000.
- [2] Gardiner C. and Zoller P., *Quantum Noise* (Springer Series in Synergetics, Berlin Heidelberg New York) 2004.
- [3] Diehl S., Micheli A., Kantian A., Kraus B., Büchler H. P. and Zoller P., *Nature Physics* **4** (2008) 878.
- [4] Diehl S., Rico E., Baranov M. A. and Zoller P., *Nature Physics* **7** (2011) 971.
- [5] Verstraete F., Wolf M. M. and Cirac J. I., *Nature Physics* **5** (2009) 633.
- [6] Kastoryano M. J., Reiter F. and Sørensen A. S., *Phys. Rev. Lett.* **106** (2011) 090502.
- [7] Krauter H., Muschik C. A., Jensen K., Wasilewski W., Petersen J. M., Cirac J. I. and Polzik E. S., *Phys. Rev. Lett.* **107** (2011) 080503.
- [8] Albiez M., Gati R., Fölling J., Hunsmann S., Cristiani M. and Oberthaler M. K., *Phys. Rev. Lett.* **95** (2005) 010402.
- [9] Gross C., Zibold T., Nicklas E., Estève J. and Oberthaler M. K., *Nature* **464** (2010) 1165.
- [10] Bakr W. S., Gillen J. I., Peng A., Foellin S. and Greiner M., *Nature* **462** (2009) 74.
- [11] Sherson J. F., Weitenberg C., Endres M., Cheneau M., Bloch I. and Kuhr S., *Nature* **467** (2010) 68.
- [12] Gericke T., Würtz P., Reitz D., Langen T. and Ott H., *Nature Physics* **4** (2008) 949.
- [13] Würtz P., Langen T., Gericke T., Koglbauer A. and Ott H., *Phys. Rev. Lett.* **103** (2009) 080404.
- [14] Bollinger J. J., Itano W. M., Wineland D. J. and Heinzen D. J., *Phys. Rev. A* **54** (1996) R4649.
- [15] Giovannetti V., Lloyd S. and Maccone L., *Science* **306** (2004) 1330.
- [16] Jaksch D., Bruder C., Cirac J. I., Gardiner C. W. and Zoller P., *Phys. Rev. Lett.* **81** (1998) 3108.
- [17] Brazhnyi V. A., Konotop V. V., Pérez-García V. M. and Ott H., *Phys. Rev. Lett.* **102** (2009) 144101.
- [18] Witthaut D., Trimborn F., Hennig H., Kordas G., Geisel T. and Wimberger S., *Phys. Rev. A* **83** (2011) 063608.
- [19] Trimborn F., Witthaut D., Hennig H., Kordas G., Geisel T. and Wimberger S., *Eur. Phys. J. D* **63** (2011) 63.
- [20] Anglin J., *Phys. Rev. Lett.* **79** (1997) 6.
- [21] Trujillo-Martinez M., Posazhennikova A. and Kroha J., *Phys. Rev. Lett.* **103** (2009) 105302.
- [22] Pichler H., Daley A. J. and Zoller P., *Phys. Rev. A* **82** (2010) 063605.
- [23] Gerbier F. and Castin Y., *Phys. Rev. A* **82** (2010) 013615.
- [24] Barmettler P. and Kollath C., *Phys. Rev. A* **84** (2011) 041606.
- [25] Kepesidis K. and Hartmann M. J., *Phys. Rev. A* **85** (2012) 063620.
- [26] Dalibard J., Castin Y. and Mølmer K., *Phys. Rev. Lett.* **68** (1992) 580.
- [27] Sinatra A., Lobo C. and Castin Y., *J. Phys. B: At. Mol. Opt. Phys.* **35** (2002) 3599.
- [28] Trimborn F., Witthaut D. and Wimberger S., *J. Phys. B: At. Mol. Opt. Phys.* **41** (2008) 171001.
- [29] Witthaut D., Trimborn F. and Wimberger S., *Phys. Rev. Lett.* **101** (2008) 200402; *Phys. Rev. A* **79** 2009033621.
- [30] Campbell D. K., Flach S. and Kivshar Y. S., *Phys. Today* **467** (2004) 57.
- [31] Ng G. S., Hennig H., Fleischmann R., Kottos T. and Geisel T., *New J. Phys.* **11** (2009) 073045.
- [32] Afek I., Ambar O. and Silberberg Y., *Science* **328** (2010)

- 879.
- [33] Trimborn F., Witthaut D. and Korsch H. J., Phys. Rev. A **77** (2008) 043631; Phys. Rev. A **79** (2009) 013608.
 - [34] Milburn G. J., Corney J., Wright E. M. and Walls D. F., Phys. Rev. A **55** (1997) 4318.
 - [35] Smerzi A., Fantoni S., Giovanazzi S. and Shenoy S. R., Phys. Rev. Lett. **79** (1997) 4950.
 - [36] Sias C., Zenesini A., Lignier H., Wimberger S., Ciampini D., Morsch O. and Arimondo E., Phys. Rev. Lett. **98** (2007) 120403.
 - [37] Peik E., Dahan M. B., Bouchoule I., Castin Y. and Salomon C., Phys. Rev. A **55** (1997) 2989.
 - [38] Kordas G., Wimberger S. and Witthaut D., in preparation 2012.
 - [39] Sørensen A. S., Duan L.-M., Cirac, J. I. and Zoller P., Nature **409** (2001) 63
 - [40] Regensburger A., Bersch C., Hinrichs B., Onishchukov G., Schreiber A., Silberhorn C. and Peschel U., Phys. Rev. Lett. **107** (2011) 233902.